Journal of Catalysis 265 (2009) 117–129

Contents lists available at ScienceDirect

Journal of Catalysis

journal homepage: www.elsevier.com/locate/jcat

Effects of H_2O and CO_2 addition in catalytic partial oxidation of methane on Rh

Brian C. Michael [a,1], Alessandro Donazzi [a,b,1], Lanny D. Schmidt [a,*]

[a] Department of Chemical Engineering and Materials Science, University of Minnesota, 421 Washington Ave. S.E., Minneapolis, MN 55455, USA
[b] Laboratorio di Catalisi e Processi Catalici, Dipartimento di Energia, Politecnico di Milano, Piazza Leonardo da Vinci 32, 20133 Milano, Italy

ARTICLE INFO

Article history:
Received 3 February 2009
Revised 11 April 2009
Accepted 22 April 2009
Available online 26 May 2009

Keywords:
Catalytic partial oxidation
Methane
Steam reforming
CO_2 reforming
Water gas shift
Spatial profile measurements
Rh
Ce
Thermodynamics

ABSTRACT

The autothermal catalytic partial oxidation (CPO) of methane was performed at short contact times (~8 ms) over three Rh-based catalysts: 5 wt% Rh/α-Al_2O_3, 5 wt% Rh/2 wt% γ-Al_2O_3/α-Al_2O_3, and 5 wt% Rh/2 wt% Ce/2 wt% γ-Al_2O_3/α-Al_2O_3. The effects of H_2O addition (10%, 20%, and 40% of the total feed) and CO_2 addition (20% and 35%) were studied over a wide range of inlet C/O ratios (0.75–1.2) by means of the capillary sampling technique. Over Rh/α-Al_2O_3 samples, spatially resolved concentration profiles revealed that the rate of CH_4 reforming is independent of the concentration of H_2O and CO_2. Differences in the product distribution followed the behavior expected from water gas shift (WGS) chemistry: in H_2O-rich tests, the production of H_2 and CO_2 increased at the expense of H_2O and CO, while the opposite was observed in CO_2-rich tests. CPO experiments with a simultaneous feed of H_2O and CO_2 (40% H_2O, 20% CO_2, 20% CH_4, C/O = 1) provided direct evidence that H_2O is the preferential co-reactant of CH_4 in reforming and that CO_2 reforming is absent. Addition of a γ-Al_2O_3 washcoat to the catalyst significantly enhanced the rate of steam reforming while revealing the limits of Rh WGS activity. Products were equilibrated for nearly all cases examined over the Ce-promoted catalyst, indicating that WGS kinetics, either forward or reverse, have an important role in the CPO mechanism, particularly with H_2O and CO_2 co-feed. The experimental results clearly illustrate the flexible nature of CPO process. They show that the H_2/CO can be varied within a wide range of values in a one-step process, and syngas production is sustainable under highly diluted conditions.

1. Introduction

In light of the growing demand and diminishing supply of fossil fuels, efficient utilization of natural gas requires flexible conversion processes to exploit reservoirs in decentralized locations. The current technology, steam reforming of methane (Eq. (1)), requires large, heat-integrated process equipment for the conversion to be economical and is not easily scaled [1].

$$CH_4 + H_2O \leftrightarrow CO + 3H_2 \quad \Delta H_r^0 = +206\ \text{kJ mol}^{-1} \tag{1}$$

$$CH_4 + \frac{1}{2}O_2 \rightarrow CO + 2H_2 \quad \Delta H_r^0 = -36\ \text{kJ mol}^{-1} \tag{2}$$

Catalytic partial oxidation (CPO, Eq. (2)) represents a valid alternative method for syngas and hydrogen production from natural gas [2]. In contrast to steam reforming, methane CPO has the advantage of being mildly exothermic and can be carried out at extremely short contact times (10^{-2} to 10^{-4} s) with autothermal reactor configurations and >90% selectivity to H_2 and CO [3]. With supported group VIII noble metal catalysts, particularly Rh and Pt, optimal performance is achieved without carbon formation [4]. These features allow for the design of simple and compact reactors with fast response to load transients, which are ideal for small- to medium-scale applications.

Although the H_2/CO ratio obtained via the CPO reaction is suitable for methanol and alkane synthesis by the Fischer-Tropsch process, different ratios are required for the synthesis of other products, such as alcohols, dimethyl ether, and acetic acid. By adding H_2O or CO_2 to the feed, a one-step adjustment of the product composition can be accomplished. Catalytic partial oxidation has also been pursued for on-board applications [5], micro-reformers [6], fuel cells [7], and catalytic burners integrated in ultra low emission gas turbines [8]. In this application, CPO is carried out under highly diluted conditions with fractions of H_2O and CO_2 amounting up to 50% and 25% v/v, respectively [9].

Understanding the effect of CO_2 and H_2O on CPO requires the analysis of the roles of steam reforming, CO_2 reforming, and water gas shift (WGS) in the reaction path. A general agreement in the literature [10–12] is that CPO proceeds through an exo-endothermic sequence of reactions. These are observed as a first step of oxidation, both partial (Eq. (2)) and total (Eq. (3)), followed by H_2 oxidation (Eq. (4)), steam reforming (Eq. (1)), and WGS (Eq. (5)).

* Corresponding author. Fax: +1 612 626 7246.
E-mail address: schmi001@umn.edu (L.D. Schmidt).
[1] These authors contributed equally to this work.

0021-9517/$ - see front matter © 2009 Elsevier Inc. All rights reserved.
doi:10.1016/j.jcat.2009.04.015

$$CH_4 + 2O_2 \rightarrow CO_2 + 2H_2O \quad \Delta H_r^0 = -803\ \text{kJmol}^{-1} \tag{3}$$

$$H_2 + \frac{1}{2}O_2 \rightarrow H_2O \quad \Delta H_r^0 = -240\ \text{kJmol}^{-1} \tag{4}$$

$$CO + H_2O \leftrightarrow H_2 + CO_2 \quad \Delta H_r^0 = -41\ \text{kJmol}^{-1} \tag{5}$$

$$CH_4 + CO_2 \leftrightarrow 2CO + 2H_2 \quad \Delta H_r^0 = +247\ \text{kJmol}^{-1} \tag{6}$$

Several authors agree that CO_2 reforming (Eq. (6)) does not partake in the scheme. By means of spatially resolved composition profiles of CH_4 CPO on Rh and Pt catalysts, Horn et al. showed that CO_2 is produced only in the presence of O_2, while its flow is unaltered in other regions where CH_4 is consumed [13,14]. Based on kinetically informative data collected at short contact time conditions over Rh-based catalysts, Donazzi et al. [12] emphasized that CO_2 reforming is a combination of steam reforming and reverse water gas shift (RWGS). The rate of CH_4 consumption, therefore, depends on the kinetics of both steam reforming and RWGS.

Other authors suggest that the mechanism of CO_2 reforming over supported noble metals is similar to that of steam reforming. Rostrup-Nielsen and Bak Hansen [14] proposed that the activation of CH_4 through pyrolysis is followed by reaction of the adsorbed C with either oxygen adatoms or hydroxyls produced by the dissociative adsorption of CO_2 and H_2O. Similarly, Wei and Iglesia [15,16] studied CH_4 reforming over a variety of catalysts, and found that the process is kinetically insensitive to the co-reactant. The authors argued that steam and CO_2 reforming are mechanistically equal, both limited by the dissociation of the first C–H bond of the CH_4 molecule, as indicated by isotopic tracer experiments.

The role of WGS in CPO with H_2O- and CO_2-rich mixtures has not been fully elucidated. Several authors agree that WGS is quasi-equilibrated with stoichiometric steam or CO_2 reforming mixtures [10,14,15,17]. However, Donazzi et al. [12] showed that WGS becomes kinetically relevant in the CPO mechanism with increasing reactant concentration. In contrast, Horn et al. [14] suggested that the WGS reaction plays a minor role in the CPO mechanism based on the constant molar flow rate of CO_2 observed with spatial profiles in the absence of O_2.

In addition to the kinetic effects of the co-feed, issues such as carbon formation and thermal effects must also be addressed to fully understand the CPO of methane. Mantzaras and coworkers [18,19] performed CPO tests at conditions pertinent to gas turbines (~8 ms contact time, 5 bar, 20% v/v CH_4 with H_2O and CO_2 dilution) with Rh-based honeycomb catalysts with different supports (ZrO_2, CeO_2–ZrO_2, and α-Al_2O_3) and observed a direct relationship between metal dispersion and catalytic performance. Decreased surface temperature, increased CH_4 conversion, and increased syngas yield were correlated with increased metal surface area. The role of the support was confined to the indirect effect of maintaining metal dispersion. Steam and CO_2 addition moderated the temperatures, but not enough to be considered adequate temperature-control agents. In agreement with these results, Schmidt and coworkers [20] showed that the addition of a washcoat (5 wt% Rh/2 wt% γ-Al_2O_3/α-Al_2O_3) brings stoichiometric CH_4 CPO feeds to thermodynamic equilibrium, significantly improves catalyst performance, and lowers surface temperatures.

A complex picture emerges from the data reported, hence interpretation of reactor performance demands consideration of a number of phenomena, including the coupling of heat and mass transfer to the overall kinetics and chemical mechanism. Complex flow patterns and large gradients in temperature and concentration further complicate the study. A thorough assessment of the reaction mechanism thus requires attention to the spatial distribution of the most relevant effects, namely where in the catalyst transport phenomena are dominant and how temperature and composition vary along the axis in relation to the pertinent chemistry. With special attention to this requirement, a comprehensive experimental investigation of the effects of H_2O and CO_2 on the CPO of CH_4 over Rh-based catalysts is presented herein.

2. Experimental

2.1. Catalyst preparation

Catalysts were prepared by impregnating monolithic alumina supports with aqueous metal precursors. Each support consisted of an 80 pores per linear inch (PPT), reticulated alumina foam cylinder measuring 17 mm in diameter and 11 mm in length (99% Al_2O_3, Hi-Tech Ceramics). Prior to impregnation, the monoliths received a 770 μm hole along the center axis with an ultrasonic drill. After cleaning with acetone and distilled water to remove drilling debris, the monoliths were treated in air at 600 °C for 6 h.

Reference catalysts (5 wt% Rh, hereafter referred to as Rh) were prepared by adding an aqueous solution of $Rh(NO_3)_3$ (~15 wt% Rh assay) dropwise to the drilled monoliths, followed by drying in air (~300 torr, 25 °C) and calcining at 600 °C for 6 h. All 5 wt% Rh/2 wt% γ-Al_2O_3 washcoat catalysts (Rh/wc) were prepared by depositing 3 μm γ-Al_2O_3 powder as an aqueous suspension to the monoliths, followed by drying, calcining, and deposition of Rh by the method mentioned above. A third formulation consisting of 5 wt% Rh/2 wt% Ce/2 wt% γ-Al_2O_3 washcoat (Rh–Ce/wc) was prepared similarly to Rh/wc; however, Ce and Rh were co-deposited from $Ce(NO_3)_3$ and $Rh(NO_3)_3$ precursors, respectively. The catalysts were reduced in situ at approximately 130 °C with a 1:10 H_2:Ar mixture prior to CPO light-off.

2.2. Experimental apparatus

The apparatus used to measure spatial profiles of species and temperature, as well as integral data, consisted of a reactor and a spatial sampling system (Fig. 1). The reactor comprised a quartz tube containing two blank monoliths surrounding a third catalytic monolith. These monoliths were wrapped tightly with aluminosilicate cloth to prevent gas bypass and slippage. Insulation was wrapped around the exterior of the reactor to minimize radial heat loss. Reactants were fed to the reactor through a temperature-controlled pre-heater to maintain a constant inlet temperature of 150 °C for all experiments. Steam was fed by pumping distilled water with an HPLC pump through a type-C ICP nebulizer (Precision Glass Blowing) into a resistively heated quartz tube. This stream was combined with the gases (fed as supplied, Airgas, CP grade) prior to entering the pre-heater.

2.3. Sampling and analysis

Gases were sampled within the monoliths by inserting a fused silica capillary (OD 550 μm) into the holes drilled through the monoliths. One end of the capillary was sealed, and a ~200 μm orifice was scribed ~35 mm from the tip. The opposite end of the capillary was connected to a microvolume tee mounted on a linear translation stage in line with the axis of the reactor. Gas was drawn through the capillary and directed to the leak valve of a quadrupole mass spectrometer (QMS, UTi 100C) and the sample loop of a gas chromatograph (GC, HP 5890, Hayesep D packed column, TCD) with a vacuum pump. The sample flow was negligibly small compared to the total flow through the reactor. The transient response and resolution of this sampling system is described in detail elsewhere [21].

Gas analysis was performed by parallel gas chromatography/mass spectrometry using Ar in the reactor feed as an internal standard. Samples were taken at the inlet and outlet of the reactor and were analyzed by GC to verify the feed and integral performance.

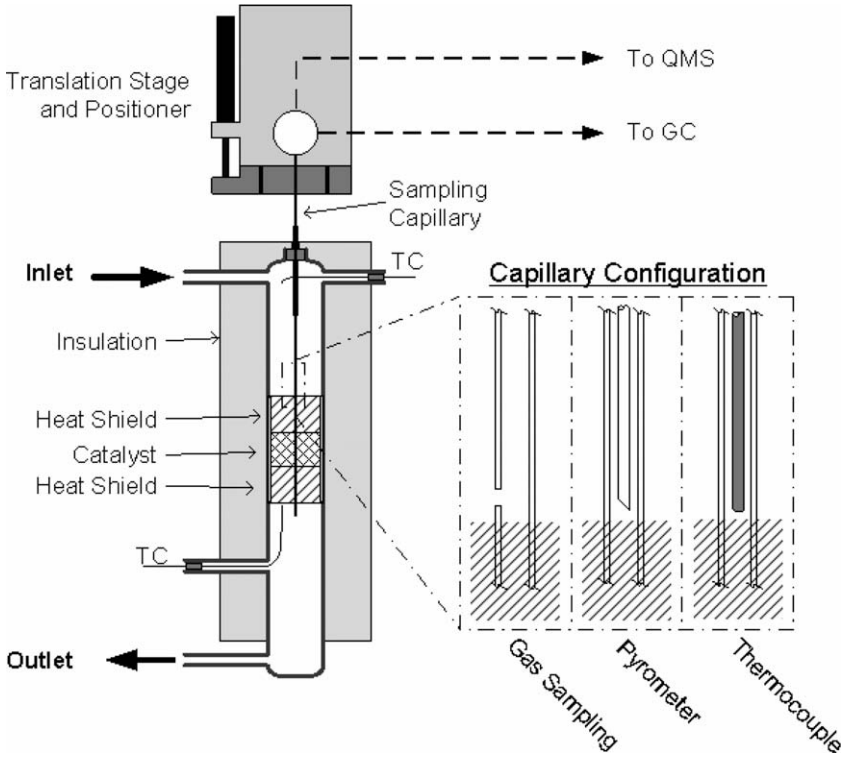

Fig. 1. CPO reactor and capillary configuration for species sampling, pyrometer, and thermocouple measurements.

Mass spectra at the inlet and outlet were matched to the GC analysis, providing local calibration of the signals at each m/z. Each analyte was quantified by a single deconvoluted m/z: 2, 15, 28, 32, 40, and 44 for H_2, CH_4, CO, O_2, Ar, and CO_2, respectively. Water was quantified by closing the O atom balance for either analysis.

To measure temperature, a sealed capillary with no orifice was inserted into the monolith, which acted as an inert sleeve for a thermocouple (type-K, 0.254" diameter) or a quartz optical fiber (0.330" diameter, 45° polished tip). The optical fiber preferentially directed radial radiation to an optical pyrometer (Mikron MI-GA 5-LO), thereby making its measurement representative of the catalyst surface temperature. Thermocouple measurements are biased toward the gas temperature owing to its physical separation from the monolith and immersion in the gas.

2.4. Operating conditions

For all data presented, the reactor feed rate was 5 slpm ($\sim 1.3 \times 10^5\ h^{-1}$GHSV), preheated to 150 °C at 1 atm. The inlet CH_4 mole fraction was held constant at 20% v/v for all experiments, while the O_2, H_2O, or CO_2 feed was varied. In this study the C/O ratio is defined with respect to only the CH_4 and O_2 feed. The inlet Ar flow made up the balance of the total flow, making these feed compositions slightly diluted compared to those in other autothermal studies where CH_4/O_2/Ar flows were varied to simulate air oxidant. The reactor closely approximated adiabatic conditions for all feed compositions studied (see Section 3.4). The atom balances of C and H closed to ±5% throughout the catalyst, with no observed carbon formation or deactivation for up to 60 h of operation. Profiles were replicated on three monoliths.

2.5. Equilibrium and performance calculations

Equilibrium compositions were calculated with constant pressure and constant enthalpy constraints by the element potential method with the STANJAN equilibrium solver available in Ref. [22]. Some comparisons make use of the C atom and H atom selectivity, which were calculated on a CH_4 feed basis:

$$S_{i,H} = \frac{\upsilon_{i,H} \cdot F_i}{4 \cdot (F^0_{CH_4} - F_{CH_4})} \tag{7}$$

$$S_{i,C} = \frac{\upsilon_{i,C} \cdot F_i}{F^0_{CH_4} - F_{CH_4}} \tag{8}$$

where $\upsilon_{i,H}$ and $\upsilon_{i,C}$ are the numbers of H atoms and C atoms in species i, respectively; F_i is the molar flow of species i, and $F^0_{CH_4}$ is the inlet molar flow of CH_4. This basis allows for selectivities greater than 100% for H_2O and CO_2 addition experiments.

3. Results

3.1. Rh catalyst: effect of H_2O addition

The effect of H_2O was investigated by adding H_2O to the reference mixture (CH_4 = 20%, C/O = 1, Ar to balance, 5 slpm). Three feed concentrations were chosen, 10%, 20%, and 40% v/v H_2O, equal to steam to carbon (S/C) ratios of 0.5, 1, and 2. Fig. 2 reports the spatial evolution of species and temperatures for these feeds and the reference CPO mixture. For each case analyzed, Table 1 lists CH_4 conversion, H_2 and CO selectivities, and the outlet temperature compared to the same values calculated at equilibrium.

The features observed in Fig. 2 are consistent with typical spatial profiles obtained for CH_4 in CPO conditions [13,21,23]. Two distinct zones are observed in the catalyst: an oxidation zone, where O_2 and CH_4 are consumed while H_2, CO, H_2O, and CO_2 are produced, and a reforming zone, where O_2 is absent and CH_4 and H_2O are consumed with steam reforming stoichiometry. As a result of the highly exothermic chemistry in the oxidation zone, a hot spot is present, which is followed by a decrease in the temperatures due to the prevailing endothermic processes in the reforming zone.

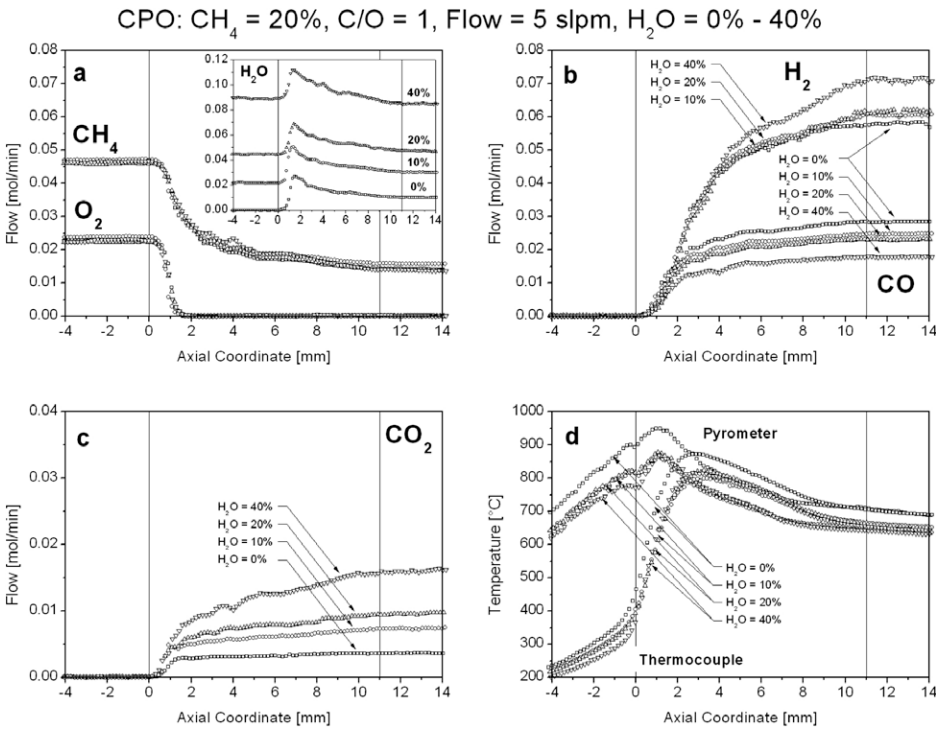

Fig. 2. Composition and temperature profiles for H_2O-rich CPO tests on 5 wt% Rh/α-Al_2O_3. CH_4 = 20 v/v%, C/O = 1, H_2O variable, Ar to balance, flow = 5 slpm. (□) H_2O = 0%; (○) H_2O = 10%; (Δ) H_2O = 20%; (▼) H_2O = 40%. Panel (a) CH_4 and O_2 molar flow rates. Panel (b) H_2 and CO molar flow rates. Panel (c) CO_2 molar flow rate. Panel (d) pyrometer and thermocouple profiles.

Table 1
CH_4 conversion, H_2 and CO selectivity, and outlet temperature for H_2O-rich tests, compared to the adiabatic equilibrium values (italics) calculated at constant P and H for T_{in} = 150 °C. Operative conditions: CH_4 = 20% v/v, H_2O = 0–40%, C/O = 1, Ar to balance, 5 slpm inlet flow, 5 wt% Rh/α-Al_2O_3.

	X_{CH_4} (%)	$S_{H_2,H}$ (%)	$S_{CO,C}$ (%)	T_{out} (°C)
H_2O = 10%	66.1	98.0	80.8	653
	83.4	*105.8*	*67.9*	*630*
H_2O = 20%	69.2	93.8	72.6	648
	82.6	*115.1*	*51.6*	*608*
H_2O = 40%	68.8	89.0	89.0	710
	83.6	*125.0*	*33.5*	*585*
H_2O = 0%	68.8	89.0	89.0	710
	79.5	*93.2*	*87.5*	*654*

Fig. 2a shows that the addition of H_2O does not affect the consumption of O_2 in the oxidation zone, and that the length of the zone is constant at ~1.8 mm for all concentrations. Furthermore, the product distribution at ~1.8 mm shows little dependence on the inlet H_2O concentration. Upon increasing the S/C ratio, the rate of CH_4 consumption is unaltered in both the oxidation and reforming zones, and results in a final conversion (~70%, Table 1) that is lower than predicted by equilibrium. In contrast, thermodynamic calculations predict an increase from 79.5% to 83.6% when H_2O inlet fraction passes from 0 to 40%.

The spatial profiles obtained for H_2O and reaction products are presented in Fig. 2a–c. An initial production of H_2O in the oxidation zone is followed by a progressive consumption downstream. For S/C ratios lower than 2, this results in net H_2O production, while at S/C of 2, a net consumption is observed. In the reforming zone, the production rates of H_2 and CO_2 progressively increase with increasing S/C, while the production of CO decreases (Fig. 2b and c).

The pyrometer measurements (Fig. 2d) shows that the catalyst surface temperature decreases to the same level regardless of the S/C ratio when H_2O is co-fed. The hot spot lowers to ~860 °C from 950 °C, and remains at 1.1 mm from the entrance. The thermocouple readings follow the same trend: the maximum goes from ~870 °C to ~815 °C and remains at 2.7 mm.

3.2. Rh catalyst: effect of CO_2 addition

Tests were performed by adding CO_2 to the reference mixture with two concentrations corresponding to CO_2/CH_4 ratios of 1 and 1.75 (20% and 35% v/v CO_2). Composition and temperature profiles are reported with the reference CPO curves (CO_2 = 0%) in Fig. 3. For each case analyzed, Table 2 lists CH_4 conversion, H_2 and CO selectivities, and the outlet temperature compared to the same values calculated at adiabatic equilibrium.

Similar to H_2O addition, increasing the CO_2/CH_4 ratio has no effect on the length of the oxidation zone (~1.8 mm) shown in Fig. 3a. The consumption of CH_4 in the oxidation zone is equal for all the three conditions, whereas in the reforming zone the addition of CO_2 results in lower consumption of CH_4. Despite the thermodynamic driving force, the outlet conversion (~65%, Table 2) is the same at 20% and 35% CO_2 and is lower than the equilibrium value.

CO_2 is always produced in the presence of O_2, as shown in Fig. 3a, and its production (evaluated as the difference between the maximum and the inlet concentration) is higher than that of the reference case when CO_2 is co-fed (~8 mmol/min vs. 3 mmol/min). In the reforming zone, two distinct behaviors can be observed. The CO_2-rich experiments display CO_2 consumption, which gives rise to a maximum that is located at the end of the oxidation zone, whereas the reference CPO mixture displays no CO_2 consumption. For the former cases, a net consumption of CO_2 is observed. The trends in H_2, CO, and H_2O profiles (Fig. 3b and c) are qualitatively opposite to those in H_2O addition when CO_2 is co-fed.

The pyrometer and thermocouple measurements shown in Fig. 3d for CO_2 addition are similar to those for H_2O addition; how-

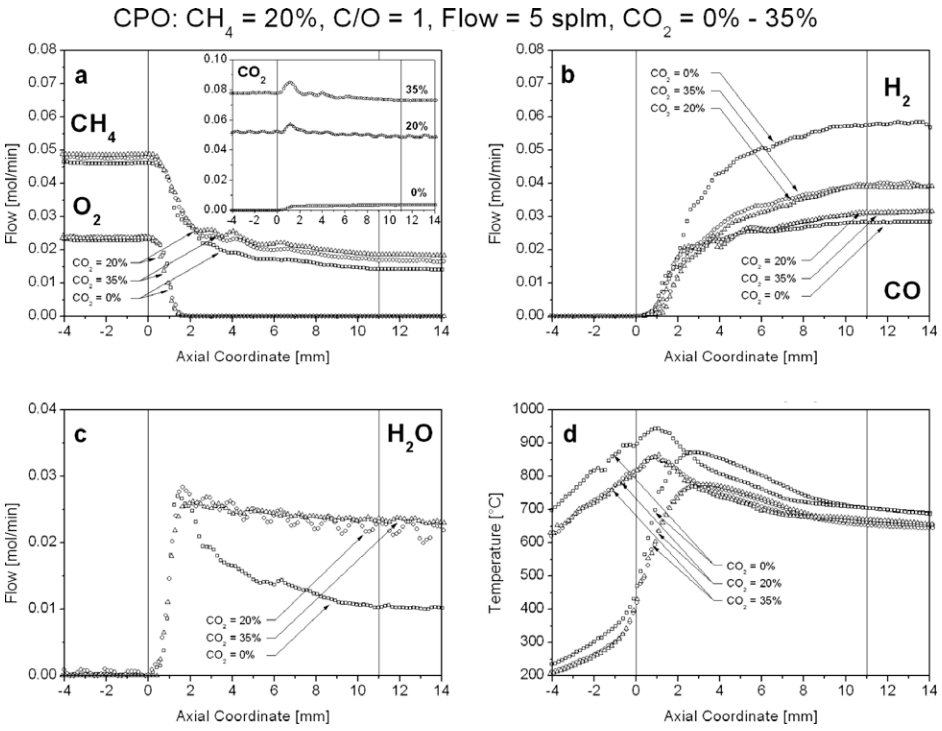

Fig. 3. Composition and temperature profiles for CO_2-rich CPO tests on 5 wt% Rh/α-Al_2O_3. CH_4 = 20 v/v%, C/O = 1, CO_2 variable, Ar to balance, flow = 5 slpm. (□) CO_2 = 0%; (○) CO_2 = 20%; (Δ) CO_2 = 35%. Panel (a) CH_4 and O_2 molar flow rates. Panel (b) H_2 and CO molar flow rates. Panel (c) H_2O molar flow rate. Panel (d) pyrometer and thermocouple profiles.

Table 2
CH_4 conversion, H_2 and CO selectivity, and outlet temperature for CO_2-rich tests, compared to the adiabatic equilibrium values (italics) calculated at constant P and H for T_{in} = 150 °C. Operating conditions: CH_4 = 20% v/v, C/O = 1, Ar to balance, CO_2 = 0–35%, 5 slpm inlet flow, 5 wt% Rh/α-Al_2O_3.

	X_{CH_4} (%)	$S_{H_2,H}$ (%)	$S_{CO,C}$ (%)	T_{out} (°C)
CO_2 = 35%	61.2	64.4	106.1	661
	69.0	*72.7*	*127.9*	*569*
CO_2 = 20%	64.5	63.7	100.7	670
	74.2	*66.4*	*120.8*	*590*
CO_2 = 0%	68.8	89.0	89.0	710
	79.5	*93.2*	*87.5*	*654*

ever, the hot spot in these cases drops from 950 °C to ~850 °C, and the thermocouple maximum decreases to ~775 °C.

3.3. Rh catalyst: effect of CO_2 and H_2O enrichment

Steam and CO_2 (40% v/v and 20% v/v, respectively) were simultaneously co-fed to the standard CPO mixture. The H_2O/CO_2 ratio of 2 is representative of the compositions obtained in exhaust recycle streams from complete combustion processes. Argon (10% v/v, 0.5 slpm) was kept as an internal standard for MS and GC measurements. Fig. 4 depicts the composition and temperature profiles obtained in the test, compared to those obtained by separately co-feeding 40% H_2O and 20% CO_2. CH_4 conversion, syngas selectivity, and the outlet temperature are listed in Table 3 with the corresponding adiabatic equilibrium values.

The CH_4 and O_2 consumption profiles are shown in Fig. 4a. The oxidation zone is slightly longer (2 mm vs. 1.8 mm) in the case of H_2O and CO_2 enrichment, but this difference is within the experimental uncertainty of the capillary technique (i.e. the position of the sampling orifice) and can be associated with the irregularities of the foam structure (bypasses and pore blockage). The rate of CH_4 consumption matches that of CO_2-rich tests; however, the final CH_4 conversion (60%) is much lower than the equilibrium limit (80%), which is comparable to equilibrium conversion for H_2O-rich tests (83.5%).

Figs. 4b and c report the spatial evolution of CO and H_2. The H_2 profile is comparable to the CO_2-rich test, even though the final production is slightly higher (45 mmol/min vs. 40 mmol/min), while the CO curve overlaps that of the H_2O-rich tests. Panels (d) and (e) report the composition profiles for H_2O and CO_2. No CO_2 consumption is observed outside the oxidation zone. Additionally, the net CO_2 production (12 mmol/min) is similar to the H_2O-rich experiment (16 mmol/min).

Thermocouple and pyrometer profiles (Fig. 4f) show that the temperatures are lower when both CO_2 and H_2O are co-fed and that the key features are shifted downstream. The hot spot passes from 860 °C to 809 °C and moves to 2 mm. The corresponding thermocouple maximum (~775 °C) shifts downstream too, but equals the maximum for CO_2-rich tests.

3.4. Rh catalyst: effect of C/O ratio

The effect of C/O ratio was investigated in the range 0.75 to 1.25, by varying the inlet concentration of O_2. Three different conditions were analyzed: CPO conditions (20% CH_4 v/v, Ar to balance, 5 slpm), H_2O-rich conditions (40% H_2O, 20% CH_4 v/v, Ar to balance, 5 slpm), and CO_2-rich conditions (20% CO_2, 20% CH_4 v/v, Ar to balance, 5 slpm). Fig. 5 shows CH_4 conversion, CO and H_2 production, and the outlet temperature as a function of C/O ratio. The corresponding equilibrium curves are also reported as dashed lines.

Upon decreasing the C/O ratio, CH_4 conversion (Fig. 5a) increases and reaches the equilibrium value at C/O of ~0.75. In the entire C/O range, the addition of H_2O has no effect on the conver-

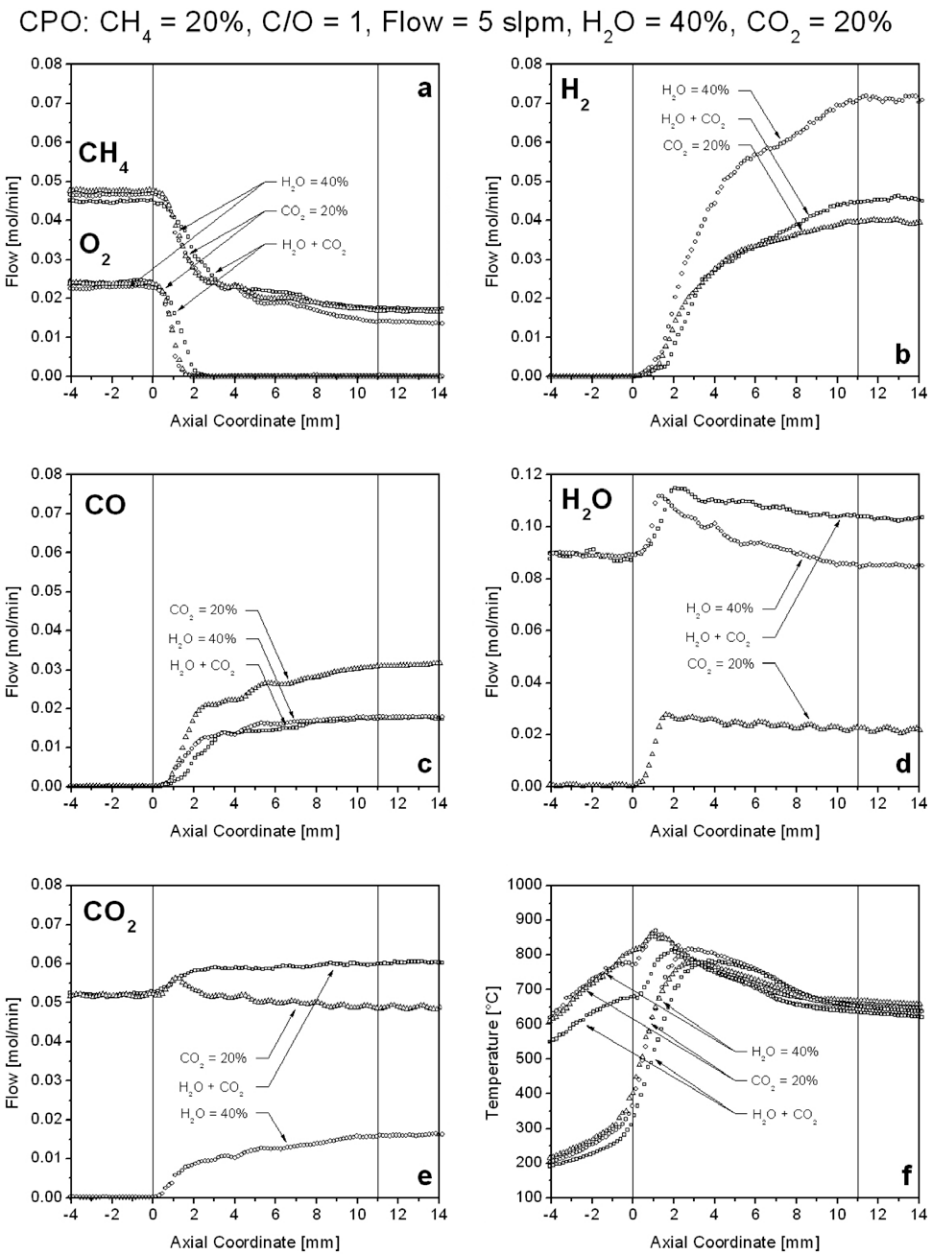

Fig. 4. Composition and temperature profiles for H_2O- and CO_2-rich CPO tests on 5 wt% Rh/α-Al_2O_3. CH_4 = 20 v/v%, C/O = 1, Ar to balance, flow = 5 slpm. (□) H_2O = 40%, CO_2 = 20%; (○) H_2O = 40%; (Δ) CO_2 = 20%.

Table 3
CH_4 conversion, H_2 and CO selectivity, and outlet temperature for the H_2O- and CO_2-rich test, compared to the adiabatic equilibrium values (italics) calculated at constant P and H for T_{in} = 150 °C. Operating conditions: CH_4 = 20%, H_2O = 40%, CO_2 = 20%, Ar 10% v/v, C/O = 1, 5 slpm inlet flow, 5 wt% Rh/α-Al_2O_3.

	X_{CH4} (%)	$S_{H2,H}$ (%)	$S_{CO,C}$ (%)	T_{out} (°C)
H_2O = 40%	59.8	90.4	62.6	638
CO_2 = 20%	*80.3*	*107.9*	*57.6*	*573*

sion of CH_4, while the addition of CO_2 decreases it. The outlet temperatures (Fig. 5b) decrease with increasing C/O. In CO_2-rich tests, the temperatures only vary within 100 °C and are nearly constant at C/O ⩾ 1. For all C/O > 0.75, the outlet temperatures are higher than the adiabatic equilibrium temperature, and in all cases, the difference between the experimental and the adiabatic temperature increases with decreasing CH_4 conversion.

The H_2 (Fig. 5c) and CO (Fig. 5d) values show a monotonically decreasing trend with increasing C/O ratio. Hydrogen production is consistently below the adiabatic level, while CO is above the equilibrium value for H_2O-rich conditions. In CO_2-rich tests with C/O ⩾ 1, the outlet CO molar flow rate matches that of the reference CPO, similar to what is observed in Fig. 3b.

Temperature profiles collected for these experiments are depicted in Fig. 6. The addition of H_2O and CO_2 results in lower temperatures than CPO tests performed at the same C/O level, while the general trend of decreased average temperature with increasing C/O is observed for all feeds. Average temperatures decrease rapidly from 0.75 < C/O < 0.8 and less rapidly for smaller concen-

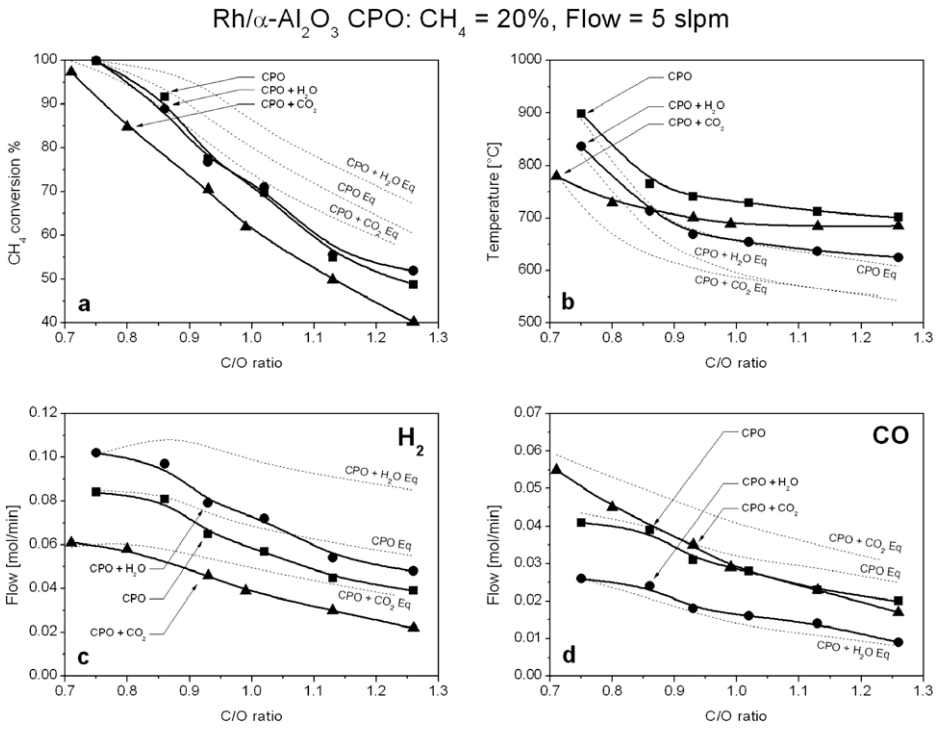

Fig. 5. Effect of the C/O ratio on 5 wt% Rh/α-Al_2O_3. (■) $CH_4/O_2/Ar$ = 20/10/70% v/v; (●) $CH_4/O_2/H_2O/Ar$ = 20/10/40/30% v/v; (▲) $CH_4/O_2/CO_2/Ar$ = 20/10/23/47% v/v. Dashed lines: equilibrium. Flow = 5 slpm. Panel (a) CH_4 conversion. Panel (b) outlet temperature. Panel (c) H_2 molar flow rate. Panel (d) CO molar flow rate.

trations of O_2. The cooling is particularly pronounced in the oxidation zone: the hot spot drops from 1060 °C to 830 °C in CPO tests, from 980 °C to 730 °C in H_2O-rich tests, and 1000 °C to 790 °C in CO_2-rich tests. Thermocouple readings follow the same qualitative trends as the pyrometer readings. In all cases, thermal equilibrium is reached in the last 2 mm of the monolith.

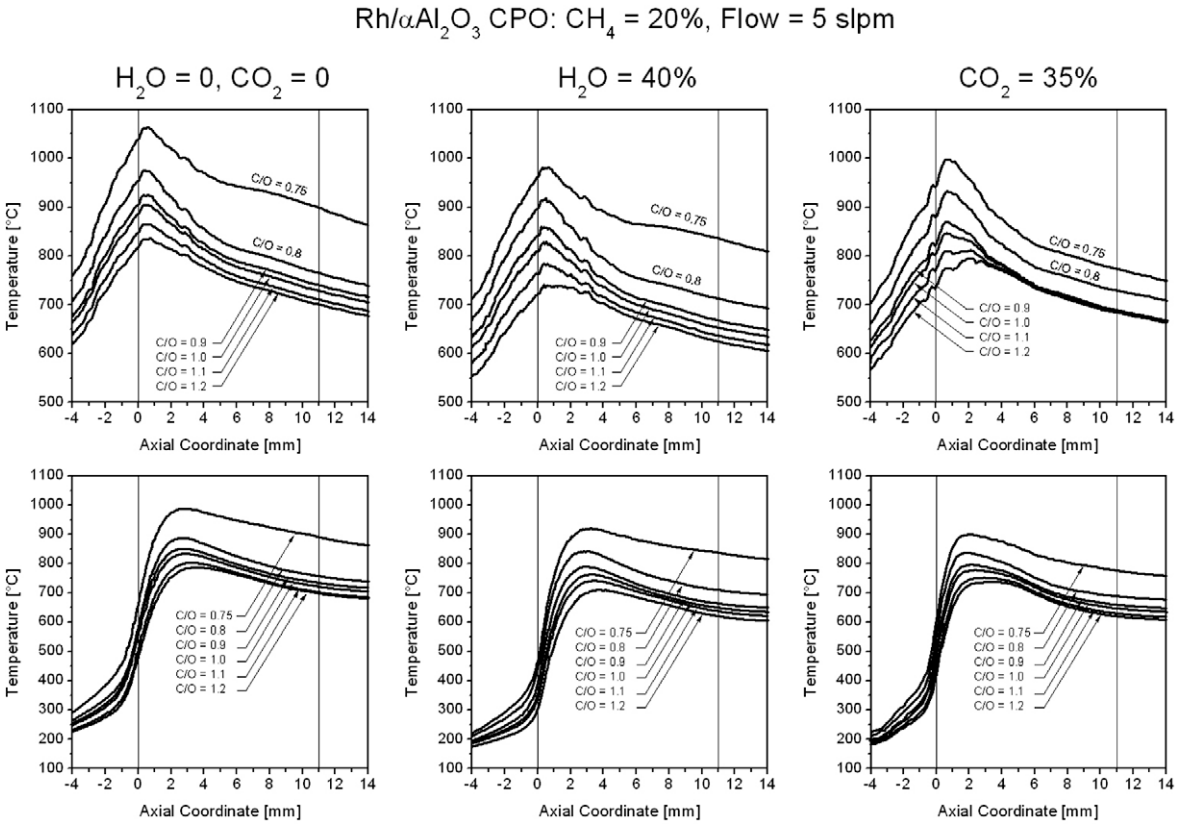

Fig. 6. Pyrometer (top) and thermocouple (bottom) temperature profiles for varying C/O ratio on 5 wt% Rh/α-Al_2O_3.

The thermal efficiency, α, of the reactor is an indication of how closely the reactor achieves adiabatic operation and is defined as:

$$\alpha = \frac{T_{ad}^{\exp} - T_{in}}{T_{ad}^{calc} - T_{in}} \tag{9}$$

where T_{in} is the inlet temperature of the gases, and $T_{ad}^{\exp}$ is the measured temperature at the outlet of the monolith. The adiabatic temperature of the exit mixture, T_{ad}^{calc}, is calculated from the following equation:

$$\dot{H}_{in}(T_{in}, \vec{n}_{in}) = \dot{H}_{out}(T_{ad}^{calc}, \vec{n}_{out}) \tag{10}$$

where $\vec{n}_{in}$ and $\vec{n}_{out}$ are the vectors of inlet and outlet molar flow rates of the species as measured by the GC. $\dot{H}_{in}$ and $\dot{H}_{out}$ are the enthalpies of the inlet and outlet gas mixtures. Based on these calculations, the efficiency is in the satisfactory range of 0.85–1, which is similar to that reported in the literature for similar CPO applications [24].

3.5. Rh/wc catalyst: effect of C/O ratio

In order to evaluate the impact that higher metal surface area has on the CPO process, a 2 wt% washcoat of 3 μm γ-Al_2O_3 particles was added to the α-Al_2O_3 foam prior to impregnation with the $Rh(NO_3)_3$ precursor. The integral results for feeds identical to the Rh sample are discussed in the present work. The spatial profiles of standard CPO tests over Rh/wc catalysts are reported elsewhere [20].

Fig. 7a shows that washcoat addition brings the CH_4 conversion to the equilibrium value both in CPO and in CO_2-rich tests at all C/O ratios. In contrast, the conversion of CH_4 is not affected by the introduction of H_2O in the mixture, similar to what is observed over the Rh catalyst (Fig. 2a). The outlet temperatures are reported in Fig. 7b. For CPO mixtures, the temperatures match the adiabatic equilibrium temperature within 10 °C, in agreement with the adiabatic behavior of the reactor. In the case of CO_2-rich mixtures, temperatures depart from equilibrium (~30–40 °C) for C/O ⩾ 1.1, where CH_4 conversions are lower than equilibrium. Temperatures are within 20 °C of the adiabatic equilibrium temperature for H_2O-rich mixtures, although the CH_4 conversion deviates from equilibrium.

Exit molar flow rates of H_2 and CO are reported in Fig. 8c and d. Under every condition, H_2 production has a maximum at C/O = 0.85, while CO production follows a monotonically decreasing trend. The H_2 and CO flow rates are at equilibrium for the reference CPO mixture. The H_2O-rich mixtures show a significant underproduction of H_2, accompanied by overproduction of CO. Conversely, in CO_2-rich tests, CO is under-produced and H_2 is higher than equilibrium. For the latter tests, the ratio between the deficit in H_2 and the deficit in CO (both evaluated as the difference between the experimental and the equilibrium values) is always ~1.

For each test in Fig. 7, temperature profiles are reported in Fig. 8. Average temperatures decrease with increasing C/O ratio like the Rh sample, but the corresponding hot spots are sharper, and located closer to the inlet. Moreover, the hot spot temperature range is more pronounced with Rh samples (1040 °C to 785 °C in CPO tests, 970 °C to 690 °C in H_2O-rich tests, and 950 °C to 725 °C in CO_2-rich tests). Downstream of the hot spot, a steep gradient is observed, which persists for the following 2 mm, followed by a steady decrease to the outlet temperature. Regardless of C/O, the addition of CO_2 or H_2O brings the average reactor temperature to lower levels than without.

3.6. Rh–Ce/wc catalyst: effect of C/O ratio

Cerium (2 wt%) and Rh (5 wt%) were co-impregnated on a washcoated monolith (2 wt% γ-Al_2O_3) in order to investigate the role of Ce in the activity of the system. The effect of the C/O ratio was studied at the same operating conditions adopted for Rh and

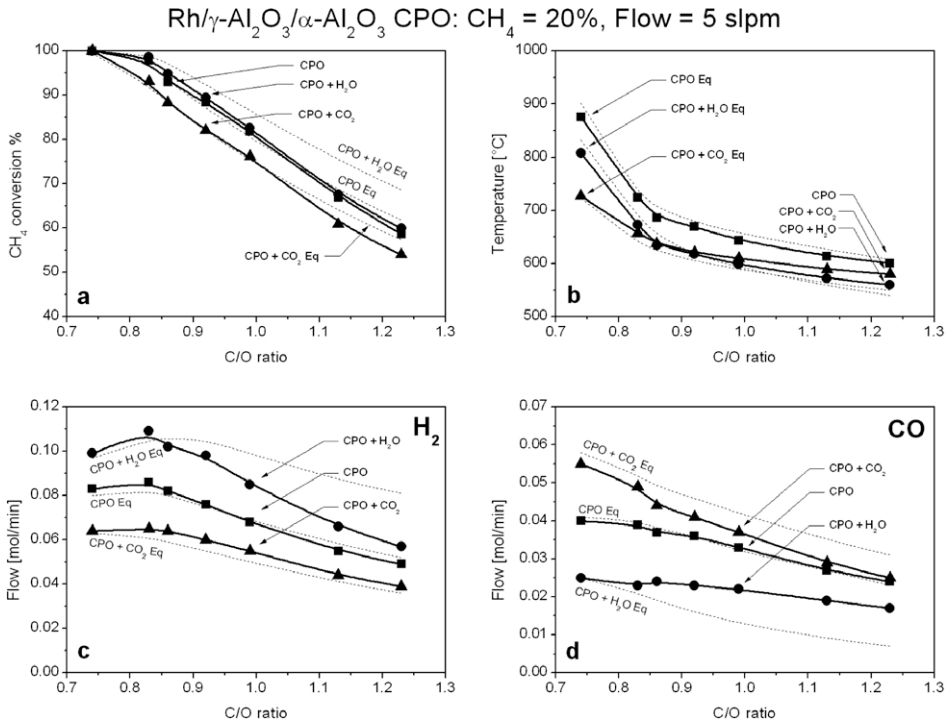

Fig. 7. Effect of the C/O ratio on 5 wt% Rh/2 wt% γ-Al_2O_3/α-Al_2O_3. (■) $CH_4/O_2/Ar$ = 20/10/70% v/v; (●) $CH_4/O_2/H_2O/Ar$ = 20/10/40/30% v/v; (▲) $CH_4/O_2/CO_2/Ar$ = 20/10/23/47% v/v. Dashed lines: equilibrium. Flow = 5 slpm. Panel (a) CH_4 conversion. Panel (b) outlet temperature. Panel (c) H_2 molar flow rate. Panel (d) CO molar flow rate.

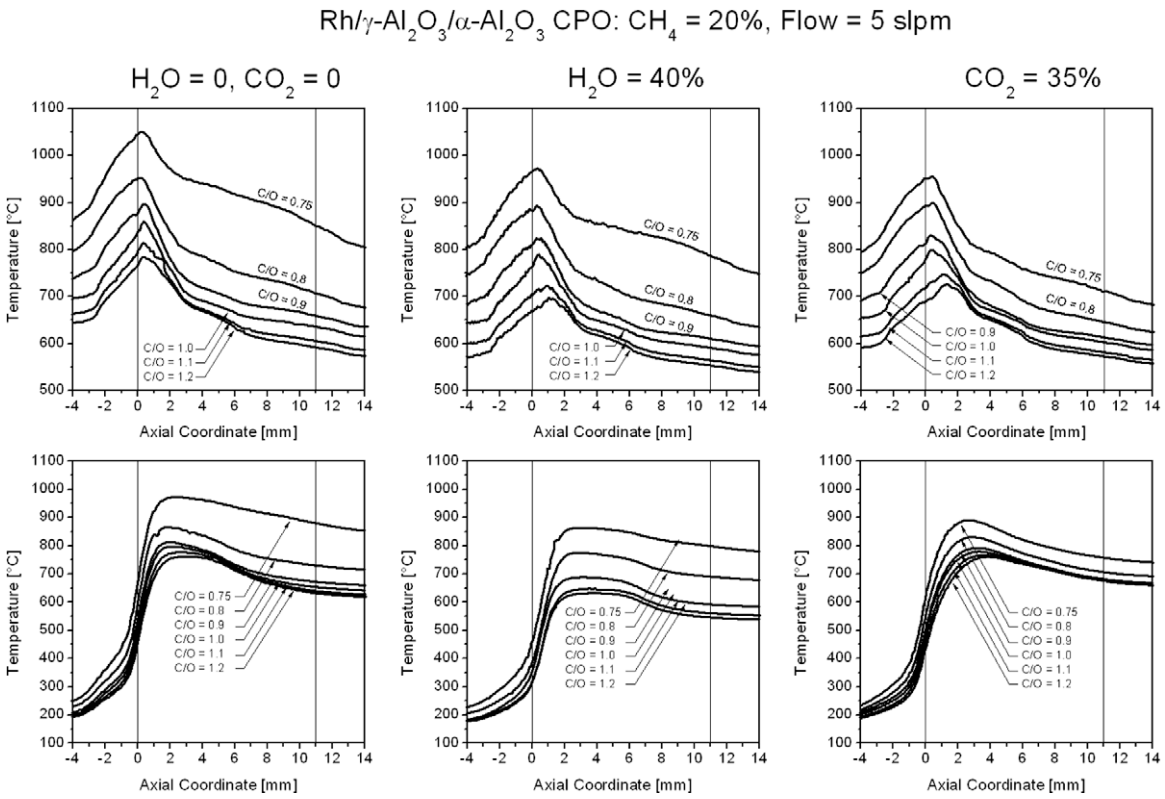

Fig. 8. Pyrometer (top) and thermocouple (bottom) temperature profiles for varying C/O ratio on 5 wt% Rh/2 wt% γ-Al_2O_3/α-Al_2O_3.

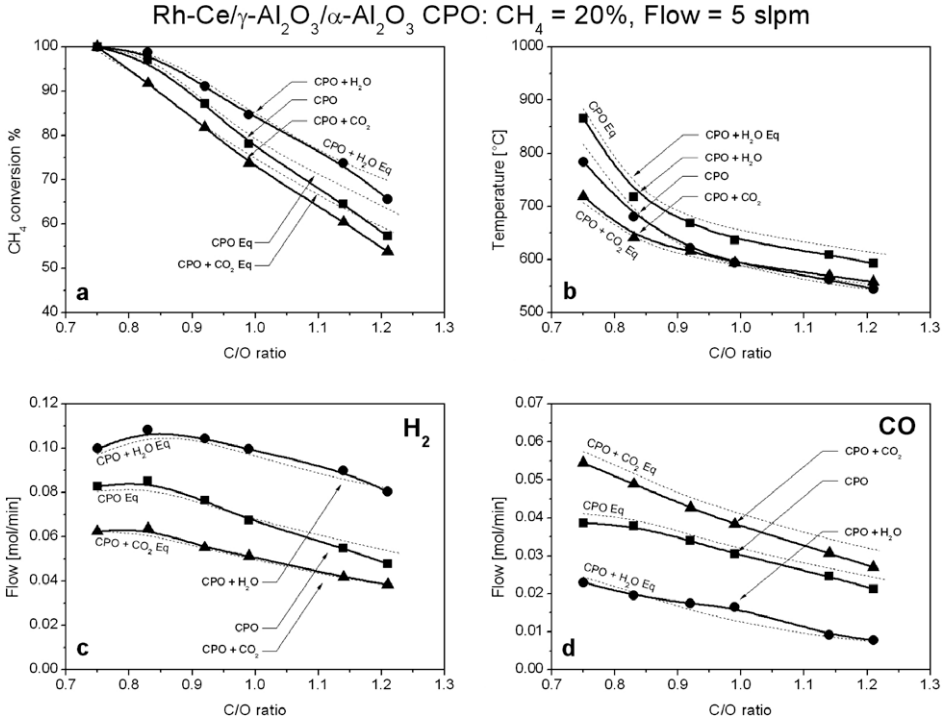

Fig. 9. Effect of the C/O ratio on 5 wt% Rh/2 wt% Ce/ 2 wt% γ-Al_2O_3/α-Al_2O_3. (■) $CH_4/O_2/Ar$ = 20/10/70% v/v; (●) $CH_4/O_2/H_2O/Ar$ = 20/10/40/30% v/v; (▲) $CH_4/O_2/CO_2/Ar$ = 20/10/23/47% v/v. Dashed lines: equilibrium. Flow = 5 slpm. Panel (a) CH_4 conversion. Panel (b) outlet temperature. Panel (c) H_2 molar flow rate. Panel (d) CO molar flow rate.

Rh/wc monoliths. For each mixture (CPO, H_2O-rich, and CO_2-rich), CH_4 conversion, outlet temperature, and the production of H_2 and CO as a function of the C/O ratio are depicted in Fig. 9.

In all cases examined, the addition of Ce brings the system to equilibrium within the experimental uncertainty. In contrast to Rh/wc, CH_4 conversion over Rh–Ce/wc (Fig. 9a) equilibrates under

H_2O-rich conditions. In the case of CPO and CO_2-rich mixtures, the curves match those obtained over Rh/wc. Correspondingly, the outlet temperatures (Fig. 9b) and the production of syngas (Fig. 9c and d) follow the trends predicted by thermodynamics.

4. Discussion

The data presented in the previous section result from the coupling of multiple phenomena. Consequently, the interpretation of reactor performance demands consideration of transport effects, equilibrium limitations, and chemical kinetics. Chemical effects will be analyzed in terms of molecular reactions, considering a scheme of CH_4 CPO that accounts for total oxidation, steam reforming, and WGS, both forward and reverse, which is a common approach in the literature [10–13]. In some parts of the discussion, activity is expressed in terms of the molar extents of these reactions, which have been fitted to the experimental outlet data.

4.1. Effect of H_2O and CO_2 addition on temperature and transport

The spatial profiles collected at C/O = 1 for H_2O- and CO_2-rich tests (Figs. 2a and 3a) show that the O_2 consumption curves have the same length and shape regardless of inlet fraction of H_2O and CO_2. This agrees well with the governing role of O_2 mass transport in the oxidation zone [8,11,23,24], and with the recent findings of Horn et al. [13], who showed that the length of the oxidation zone is fixed for a constant flow rate over a wide range of C/O ratios (i.e. of O_2 partial pressure) on Rh-based catalysts in the CPO of CH_4.

The insensitivity to co-feed type and amount can be rationalized by considering the functional dependence of the O_2 mass transfer coefficient on the properties of the bulk fluid. It has been shown in [13] that the mass transfer correlation given by Giani et al. [25] can be used with 80 ppi foams. For this system, therefore, the following equation for the Sherwood number can be applied:

$$Sh = 0.91 \cdot Re^{0.43} \cdot Sc^{1/3} \tag{11}$$

The Sherwood number relates the strut diameter d_s, the molecular diffusivity D_m, and the mass transfer coefficient k_m by:

$$Sh = \frac{k_m \cdot d_s}{D_m} \tag{12}$$

The Reynolds number and Schmidt number are defined respectively by:

$$Re = \frac{u \cdot \rho \cdot d_s}{\mu} \tag{13}$$

$$Sc = \frac{\mu}{\rho \cdot D_m} \tag{14}$$

By substituting Eqs. (12)–(14) into (11), the dependence of the mass transfer coefficient on the fluid properties is obtained:

$$k_m \sim u^{0.43} \cdot d_s^{-0.57} \cdot (\rho/\mu)^{0.1} \cdot D_m^{2/3} \tag{15}$$

The velocity u and the strut diameter d_s are fixed, and the difference in density ρ and viscosity μ of the fluid owing to CO_2 and H_2O substitution for Ar only weakly affects k_m. Additionally, D_m, the molecular diffusivity of O_2 in the mixture as predicted by the Fuller–Schettler–Giddings correlation [26], weakly varies with co-feed (Table 4). Hence, the individual addition of either H_2O or CO_2 negligibly affects O_2 transport properties, so the oxidation zone is not expected to deviate appreciably. If the length of the oxidation zone observed in the reference CPO profile is rescaled according the ratios of $1/k_m$ predicted by Eq. (15), then the differences expected for all the examined feeds are within the experimental uncertainty (see also Table 4).

Table 4
Selected fluid properties and predicted oxidation zone length for various feed mixtures calculated at P = 1 atm, T = 700 °C. Operating conditions: 20% CH_4, C/O = 1, 5 slpm inlet flow, 5 wt% Rh/α-Al_2O_3.

Feed mixture	D_m[a] ($cm^2\ s^{-1}$)	$D_m^{2/3}$ ($cm^{4/3}\ s^{-2/3}$)	Z_{ox}[b] (mm)	$C_{p,mix}$ ($J\ mol^{-1}\ K^{-1}$)
CPO	1.80	1.48	1.80[c]	32.1
H_2O = 10%	1.85	1.51	1.77	34.1
H_2O = 20%	1.91	1.54	1.73	36.0
H_2O = 40%	2.03	1.60	1.66	40.0
CO_2 = 20%	1.71	1.43	1.86	38.7
CO_2 = 35%	1.65	1.40	1.90	43.6
H_2O = 40%, CO_2 = 20%	1.92	1.55	1.72	46.6

[a] Oxygen mixture diffusivity calculated from Blanc's Law using binary diffusion coefficients estimated from the Fuller–Schettler–Giddings correlation.
[b] Calculated by scaling the measured reference run oxidation zone length by the calculated D_m according to Ref. [13].
[c] Measured from CPO profile.

In H_2O- and CO_2-rich tests, an important consequence of mass transfer limitation on oxygen is that CH_4 also has a constant consumption profile in the oxidation zone. Hence, the amount of exothermic heat released is almost the same in both cases. Given that the heat capacities of CO_2 and H_2O are higher than that of Ar, the gas and surface temperatures are expected to decrease with respect to the reference conditions because the overall system heat capacity is higher (Table 4). It is important to note that heat capacity alone cannot be responsible for the observed differences upon the addition of CO_2 or H_2O. The change in temperatures is coupled to adiabatic operation, hence the product distribution must be considered when comparing the temperatures as well.

Downstream of the oxidation zone, the species and the temperature profiles indicate a net endothermic process. Since the only source of heat in these reactors is that released by the oxidative chemistry, efficient heat transport to the endothermic zone is essential for maintaining high temperatures and reaction rates. At steady state, a balance between heat transfer to the reforming zone and heat consumption by reforming must be observed, which requires that surface temperatures be lower than gas temperatures in the absence of high solid conduction. Therefore, the observed differences between thermocouple and pyrometer profiles (i.e. convective driving force) in the reforming zone indicate that heat transfer from the gas phase to the surface is kinetically important. Since the observed driving force is not significantly different for the CO_2- and H_2O-rich runs compared to the reference, the data (Figs. 2d and 3d) indicate that H_2O or CO_2 co-feed does not appreciably affect the convective heat transfer.

The pyrometer and thermocouple profiles (Figs. 2d and 3d) do not deviate appreciably with inlet fraction when either H_2O or CO_2 are co-fed. This is a complex result, and it is likely that a number of factors contribute to the behavior. First, the thermal efficiency of the reactor used herein is high: hence, the similar temperatures observed for the various inlet compositions imply that there is a close agreement between the change in the heat capacity of the product mixture and the enthalpy change from reaction upon variation in the co-feed. Second, since the pyrometer is biased toward the surface temperature, equal profiles suggest that the overall surface reaction is thermally similar for each co-feed inlet fraction, which is consistent with the relatively constant reforming behavior observed in Fig. 2a. Finally, the effects of changing mixture heat capacity should be most pronounced in the gas phase, and therefore observable in the thermocouple measurement. However, this measurement is less sensitive to small differences in local temperature since it is subject to axial conduction and radiation at high temperatures. A reasonable experimental error of ±5% could obscure these effects. A practical observation

is that H_2O and CO_2 addition only slightly changes the operating temperatures, and the balance between oxidation and reforming largely governs the heat distribution.

With an account of the temperature and transport effects for H_2O and CO_2 addition established, a discussion of the kinetic effects of H_2O and CO_2 addition for the Rh catalyst is presented next.

4.2. Effect of H_2O and CO_2 addition on product distribution

For the data depicted in Figs. 2 and 3 to be kinetically relevant, they must be sufficiently far from equilibrium and free of heat loss artifacts. Tables 1 and 2 show that the CH_4 conversion is lower than that predicted by thermodynamics, and the outlet temperatures are up to 100 °C higher than the equilibrium temperature, indicating a lack of endothermic reforming activity. The reaction does not reach equilibrium for any level of co-feed on the Rh catalyst. This condition, coupled with the high thermal efficiency of the reactor, indicates that the data are kinetically informative.

The addition of H_2O to the feed has a negligible effect on the steam reforming rates. Spatial profiles (Fig. 2a) indicate that CH_4 conversion profiles are constant with increasing H_2O content, contrary to the thermodynamic prediction. The insensitivity of the steam reforming rate to the H_2O concentration has been observed in isothermal kinetic studies [12,15] and in autothermal reactors [27], and suggests that the steam reforming rate has a zeroth order dependence on H_2O. The addition of H_2O affects the product distribution only through the WGS: at equal CH_4 conversion, H_2 production increases at the expense of CO production (Fig. 2b). Therefore, by varying H_2O content, it is possible to modulate the H_2/CO ratio at the outlet with no influence on CH_4 consumption.

Unlike H_2O addition, the addition of CO_2 decreases CH_4 conversion in accordance with the decrease predicted by equilibrium. Additionally, CO_2 addition affects the product distribution by WGS chemistry. The spatial profiles (Fig. 3c and d) show that CO and H_2O production increase while H_2 production decreases upon increasing CO_2 feed content to 20% (that is, a 10-fold increase of the average CO_2 concentration in the catalysts). However, no appreciable difference in product distribution and reactant conversion is observed upon increasing the concentration of CO_2 from 20% to 35% v/v (a 1.75-fold increase). This observation suggests that the rate of RWGS is a weak function of the CO_2 concentration for CO_2 concentrations greater than 20%.

Although the oxidation zone is primarily characterized by chemistry limited by O_2 transport, reforming and water gas shift reactions have a role in the chemical pathway that occurs in this region. Indeed, differences in the product distribution at the end of the oxidation zone can be observed, which should be primarily attributed to WGS, due to the insensitivity of reforming to the co-reactant nature and amount. Furthermore, in this zone the ratio of changes in H_2O and CO_2 production is 1:1, in line with the stoichiometry of WGS. However, since the overall oxidation zone stoichiometry closely matches partial oxidation reactions, it is clear that O adatoms are the preferred co-reactants for CH_4 pyrolysis products.

4.3. Effect of the C/O ratio

Over the Rh catalyst, integral data (Fig. 5) confirm that the features observed with spatial profiles persist over the entire C/O range examined. The system reaches equilibrium only at C/O $\leqslant$ 0.75. At this low C/O regime, the temperature increases more rapidly and selectivity to CO_2 and H_2O (deep combustion products) is favored. Since peak pyrometer temperatures change more than outlet temperatures with C/O (Fig. 6), it can be reasoned that the effect of C/O is more confined to the chemistry in the oxidation zone. Consequently, the reforming rate near the oxidation zone (where CH_4 concentration is still high) is enhanced and less dependent on heat transfer from the gas phase, resulting in equilibrium conversion. Therefore, any heat transfer limitation that may exist downstream is less important when temperatures near the oxidation zone are sufficiently high.

To gain further insight into the relative importance of CO_2 and H_2O reforming, a comparison between the dual co-feed test (20% CO_2, 40% H_2O) and individual H_2O-rich and CO_2-rich tests is provided next. These data, presented in Fig. 4, are also relevant to exhaust gas-diluted CPO systems such as those in the AZEP process [9].

4.4. The importance of CO_2 reforming

The results of the combined addition test are consistent with those reported by Eriksson et al. under similar conditions (~8 ms contact time, 20% v/v CH_4, 5 bar, Rh/α-Al_2O_3 honeycomb catalysts) [18,19]: CH_4 conversion and syngas selectivity do not reach equilibrium, a moderate net production of H_2O and CO_2 is observed, and the outlet temperature is ~70 °C higher than adiabatic.

In H_2O + CO_2 co-feed experiments, the oxidation zone length is almost equal to that of CO_2-rich tests (0.2 mm longer); however, the shape of the oxygen consumption curve is also slightly different. Although these differences are within the experimental uncertainty of the capillary sampling technique (±0.3 mm) and can be attributed to bulk fluid properties of the reacting mixtures (Section 4.1), the possibility of rate inhibition by the large co-feed concentration should be considered. Mass transfer limitation in oxygen implies that the Rh surface is clean; however, if selective adsorption of H_2O and CO_2 occurs, then available sites for O_2 adsorption would decrease along with the rate of O_2 conversion. This would lengthen the oxidation zone and possibly alter the product distribution. Since these effects are not pronounced in Fig. 4, we cannot conclude the occurrence of preferential CO_2 or H_2O adsorption.

The addition of both CO_2 and H_2O shifts the hot spot downstream and modifies the temperature evolution in the reforming zone with respect to H_2O- and CO_2-rich tests. It is speculated that these effects are associated to the increased IR absorptivity of the gas mixture, which could affect radiative heat transfer, more likely than being associated with the reforming chemistry. Nonetheless, further quantitative analysis is needed to fully understand such complex results.

In the reforming zone, CH_4 conversion is equal to that measured in the CO_2-rich run (Fig. 4a). Additionally, the net H_2O consumed in the two runs is almost the same. However, in the CO_2 + H_2O test, H_2O consumption is observed in the absence of CO_2 consumption (Fig. 4d and e). These data agree with the negligible role of CO_2 reforming in favor of considerably faster steam and oxy reforming of CH_4 reported by several authors [10,12,14–19], and clearly show that H_2O is the preferential co-reactant of CH_4 in reforming reactions. Thus, the reforming section of the catalyst is governed only by steam reforming and WGS chemistry, either forward or reverse, depending on the local balance of H_2O, CO_2, H_2, and CO. In the case of CO_2 + H_2O test, the 2:1 feed ratio between H_2O and CO_2 favors WGS, thereby causing higher H_2 and lower CO formation with respect to the CO_2-rich run. On the other hand, the observed consumption of CO_2 in CO_2-rich runs is associated only with RWGS activity, and is also responsible for the different product distribution for the two tests.

To this point, the discussion has been centered on the kinetics associated with the Rh catalyst. In the following sections, integral results for the Rh/wc and Rh–Ce/wc catalysts are used to help elucidate how steam reforming and water gas shift pathways are related for feeds rich in H_2O or CO_2.

4.5. Reforming enhancement by washcoat addition

It is widely understood that the presence of a washcoat plays a substantial role in maintaining metal dispersion and increasing surface area [28,29] for noble metal catalysts. Degenstein et al. showed that, for the same catalytic formulations used herein, there is a large difference between washcoated and non-washcoated catalysts in terms of metal particle size. Without a washcoat phase, the particle diameters range between 1 and 40 μm, whereas no particles are visible in the presence of a washcoat, indicating that the sample has a much higher dispersion [29]. The increase in CH_4 conversion shown with Rh/wc is fully in line with the increase in metal area, which increases the total number of active sites available for the reaction. In addition, increased dispersion is particularly beneficial for steam reforming since the activation of methane is a surface sensitive process [15,16], i.e. the turnover frequency increases with increased dispersion. By means of spatial profiles, we have recently shown that these effects are pronounced in autothermal CPO reactors: the oxidation zone length is unaffected, while the rate of reforming increases within the oxidation zone and results in a decrease in the hot spot from the overlap of the endothermic and exothermic chemistry [20].

Inspection of the temperature profiles for the present work (Fig. 8) reveals that the hot spot and the average temperatures decrease throughout the reactor. The hot spot moves closer to the inlet section and a steep gradient follows. These trends are evidence of an enhancement of endothermic reforming activity. In comparison to Fig. 6, the steeper slopes exhibited in Fig. 8 near the oxidation zone indicate that the same general enhancement of steam reforming occurs for CO_2 and H_2O enrichment.

The data presented in Fig. 7 shows that the increase in reforming activity brings the CH_4 conversion to the equilibrium for CO_2-rich and CPO feeds over the entire C/O range; however, the increase is not sufficient to bring the H_2O-rich test to equilibrium conversion for C/O > 0.85. The increase in activity can be seen in Table 5 by comparing the extents of steam reforming reaction for the Rh and Rh/wc catalysts.

Washcoat addition reveals an apparent limit in the WGS activity of the Rh catalysts. Despite the increase in Rh dispersion expected from washcoat addition (and indicated by the increased reforming rates), Table 5 shows that the extent of WGS (relative to the equilibrium WGS extent) is essentially equal for Rh and Rh/wc samples. For CPO conditions, WGS reaches equilibrium in agreement with literature results [10,14–17], so no difference can be expected between the two catalysts; however, the addition of CO_2 or H_2O to CPO dramatically increases the extent of WGS required to equilibrate those feeds. The product distribution shown in Fig. 7 for CO_2- and H_2O-rich feeds further indicates that this WGS extent is not met, even when Rh dispersion is increased.

Table 5
Extents of steam reforming ($\xi_p/\xi_{eq,SR}$) and water gas shift ($\xi_p/\xi_{eq,\ WGS}$) reactions normalized to the same values at equilibrium and averaged over all C/O ratios for the indicated feed and catalyst. CPO: CH_4 = 20%; CPO + H_2O: CH_4 = 20%, H_2O = 40%; CPO + CO_2: CH_4 = 20%, CO_2 = 20%; flow = 5 slpm, C/O = 1. Extents of reaction were calculated by least-squares regression of the outlet data depicted in Figs. 5, and 7, and total oxidation for O_2 consumption was assumed.

Feed mixture	$\xi_p/\xi_{eq,SR}$	$\xi_p/\xi_{eq,WGS}$
Rh		
CPO + H_2O	0.80	0.49
CPO	0.87	1.05
CPO + CO_2	0.78	0.61
Rh/wc		
CPO + H_2O	0.96	0.51
CPO	1.00	1.09
CPO + CO_2	0.98	0.73

Although the evaluation of integral reactor performance provides only a qualitative picture of the chemistry (and no direct information about mass transfer or surface phenomena), it can be hypothesized from the data in Figs. 5 and 7 that H_2O and CO_2 added to the system have only a limited influence on the surface processes intrinsic to WGS on Rh and Rh/wc catalysts. To prove this hypothesis, the same tests were conducted on the Rh–Ce/wc catalyst, which is known to be more active in WGS.

4.6. Water gas shift enhancement by Ce addition

Similar to the incorporation of a washcoat, the use of rare earth metals is also common in combustion catalysts [30], and it is generally accepted that Ce is a beneficial additive in CPO catalysts, either as a dopant or as a support [28,31]. The addition of Ce allows for the possibility of additional distinct catalytic sites (e.g. H_2O adsorption sites), and therefore additional chemical pathways. A common observation is that Ce-doped (or CeO_2-supported) noble metals are more active in water gas shift on the basis of increased turnover frequency or observed rate constant [32].

One interpretation of the role of Ce under H_2O-rich conditions is that it directly promotes the steam reforming activity [28], which increases CH_4 conversion to the equilibrium value. We have recently shown [20] that this may not be the case for the system studied herein. By comparing the same reference CPO mixture (C/O = 1, CH_4 = 20%, Ar to balance, 5 slpm), spatial profiles showed that the reforming rate increases in the order Rh/wc > Rh–Ce/wc > Rh, although the rates for Rh/wc and Rh–Ce/wc were high enough to equilibrate the products by the outlet.

The integral effects of adding 2 wt% Ce to Rh/wc samples are illustrated in Fig. 9. In all examined cases, it is evident that the addition of Ce brings the system to equilibrium. In CO_2-rich tests, the effect is confined to the product distribution, namely to a subtle enhancement of the RWGS activity of the catalyst. A more pronounced change is shown for H_2O-rich runs. Specifically, CH_4 conversion, syngas production, and outlet temperatures closely match their equilibrium values, indicating that the addition of Ce leads to an increase in average steam reforming rate as well.

Considering the general view that Ce enhances WGS, along with the data presented, an alternative explanation for the increase in steam reforming activity can be proposed based on the interaction between the WGS and steam reforming steps. By noting the kinetic irrelevance of H_2O on steam reforming, the interaction can be discussed in terms of CO concentration since it is a product of steam reforming and a reactant for WGS.

The addition of washcoat increases the reforming rate for all feeds tested; however, H_2O-rich tests do not reach equilibrium at high C/O and display insufficient WGS chemistry. While the increase in reforming activity is sufficient to bring CPO and CO_2-rich experiments close to equilibrium (which defines a lower conversion limit than for the H_2O-rich case), equilibration for H_2O-rich runs requires a route for CO conversion, i.e. WGS. By adding Ce to the catalyst, the WGS activity increases, allowing for CO conversion to CO_2, which in turn allows the reforming reaction to proceed to equilibrium. This mechanism implies that steps associated with forward WGS are also key steps in the removal of intermediates that inhibit the overall steam reforming rate. Inhibition of steam reforming by CO, for example, has been observed in other studies [10,12,14,17] and is consistent with the overall interpretation mentioned above.

Without knowledge of the composition profiles within the catalyst (that is, without the use of a spatially resolved technique), it would not have been possible to underline the decrease in steam reforming rate caused by the addition of Ce. As a consequence, a direct reforming enhancement would be the simplest interpretation of the effect of Ce on H_2O-enriched CPO.

5. Conclusions

In this work, the effects of H_2O and CO_2 on the catalytic partial oxidation of methane are analyzed for a wide range of C/O ratios over three different Rh-based catalysts. The capillary sampling technique allows for the analysis of integral reactor data with direct knowledge of the trends in temperature and species profiles within the catalyst bed. In this way, a deeper insight into CPO process is provided.

In the oxidation zone, O_2 mass transfer limits the rate of reaction, which is unaffected by H_2O and CO_2 addition as indicated experimentally by identical oxygen profiles obtained for all feed mixtures. Downstream, the reforming zone of the reactor is primarily affected by co-feed through WGS chemistry. Reforming rates are invariant to the concentration of co-reactant. By simultaneously feeding CO_2 and H_2O to the CPO reactor, it can be shown that reforming chemistry is governed by a combination of steam reforming and forward or reverse water gas shift depending on the feed composition. Therefore, in CO_2-rich conditions, apparent CO_2 reforming stoichiometry can be explained on the basis of reverse water gas shift and steam reforming activity.

On Rh catalysts, integral data show that reforming and WGS reactions are not equilibrated for C/O ratios > 0.8. However, increased deep oxidation at lower C/O values leads to higher temperatures near the oxidation zone, and consequentially raises reforming rates such that all feeds are equilibrated. Addition of γ-Al_2O_3washcoat and Ce indicates that non-equilibrium performance with the Rh catalyst is attributed to its intrinsic activity. On the Rh/wc catalyst, the rate of reforming increased for all feeds, whereas the WGS rates were only moderately affected, therefore suggesting a limit in the activity of Rh for WGS under the conditions studied. This was confirmed by adding Ce to the catalyst formulation, which resulted in equilibration of all feeds. In particular, enhancement of WGS provides a route for CO conversion in H_2O-rich tests, thereby allowing equilibrium CH_4 conversion by steam reforming.

Although the major effects of H_2O and CO_2 on the CPO of CH_4 have been explained experimentally, a few, minor effects have not been fully elucidated. To quantitatively address these issues, reactor modeling approaches are promising and could benefit directly from the data presented here. Nonetheless, by influencing WGS equilibrium, CO_2 and H_2O co-feed proves to be a simple method for adjusting the H_2/CO ratio in the CPO of CH_4.

Acknowledgment

This work was partially supported by DOE Grant DE-FG36-05GO15023.

References

[1] J.A. Moulijn, M. Makkee, A. Van Diepen, Chemical Process Technology, New York, 2001.
[2] A.P.E. York, T. Xiao, M.L.H. Green, J.B. Claridge, Catal. Rev. Sci. Eng. 49 (2007) 511.
[3] D.A. Hickman, L.D. Schmidt, J. Catal. 138 (1992) 267.
[4] A.P.E. York, T. Xiao, M.L.H. Green, Top. Catal. 22 (2003) 345.
[5] D. Neumann, M. Kirchhoff, G. Veser, Catal. Today 98 (2004) 565.
[6] J.A. Federici, D.G. Norton, T. Brüggemann, K.W. Voit, E.D. Wetzel, D.G. Vlachos, J. Power Sources 161 (2006) 1469.
[7] A.K. Chaniotis, D. Poulikakos, J. Power Sources 142 (2005) 184.
[8] M. Lyubovsky, L.L. Schmidt, M. Castaldi, H. Karim, B. Netwick, S. Etemad, R. LaPierre, W.C. Pfefferle, Catal. Today 83 (2003) 71.
[9] T. Griffin, D. Winkler, M. Wolf, C. Appel, J. Mantzaras, ASME Paper, 2004. p. 54101.
[10] M. Maestri, D.G. Vlachos, A. Beretta, G. Groppi, E. Tronconi, J. Catal. 259 (2008) 211.
[11] R. Schwiedernoch, S. Tischer, C. Correa, O. Deutschmann, Chem. Eng. Sci. 58 (2003) 633.
[12] A. Donazzi, A. Beretta, G. Groppi, P. Forzatti, J. Catal. 225 (2008) 241.
[13] R. Horn, K.A. Williams, N.J. Degenstein, A. Bitsch-Larsen, D. Dalle Nogare, S.A. Tupy, L.D. Schmidt, J. Catal. 249 (2007) 378.
[14] J.R. Rostrup-Nielsen, J.-H. Bak Hansen, J. Catal. 144 (1993) 38.
[15] J. Wei, E. Iglesia, J. Catal. 225 (2004) 116.
[16] J. Wei, E. Iglesia, J. Catal. 224 (2004) 370.
[17] M.C.J. Bradford, M.A. Vannice, Appl. Catal. A 142 (1996) 73.
[18] S. Eriksson, A. Schneider, J. Mantzaras, M. Wolf, S. Jaräs, Chem. Eng. Sci. 62 (2007) 3991.
[19] A. Schneider, J. Mantzaras, P. Jansohn, Chem. Eng. Sci. 61 (2006) 4632.
[20] A. Donazzi, B.C. Michael, L.D. Schmidt, J. Catal. 260 (2008) 270.
[21] R. Horn, K.A. Williams, N.J. Degenstein, L.D. Schmidt, Catal. Lett. 110 (2006) 169.
[22] Stanjan Chemical Equilibrium Calculation. <http://navier.engr.colostate.edu/tools/equil.html>.
[23] A. Bitsch-Larsen, R. Horn, L.D. Schmidt, Appl. Catal. A: General 348 (2008).
[24] I. Tavazzi, M. Maestri, A. Beretta, G. Groppi, E. Tronconi, P. Forzatti, AIChE J. 52 (2006) 3234.
[25] L. Giani, G. Groppi, E. Tronconi, Ind. Eng. Chem. Res. 42 (2003) 62.
[26] R.C. Reid, J.M. Prausnitz, B.E. Poling, The Properties of Gases and Liquids, McGraw-Hill, New York, 1987. p. 587.
[27] E.J. Klein, S. Tummala, L.D. Schmidt, Nat. Gas Convers. VI, Stud. Surf. Sci. Catal. 136 (2001) 245.
[28] A. Trovarelli, Catal. Rev. Sci. Eng. 38 (1996) 439.
[29] N.J. Degenstein, R. Subramanian, L.D. Schmidt, Appl. Catal. A 305 (2006) 146.
[30] H.S. Gandhi, G.W. Graham, R.W. McCabe, J. Catal. 216 (2003) 433.
[31] S. Eriksson, S. Rojas, M. Boutonnet, J.L.G. Fierro, Appl. Catal. A 326 (2007) 8.
[32] C. Wheeler, A. Jhalani, E.J. Klein, S. Tummala, L.D. Schmidt, J. Catal. 223 (2004) 191.